

Prospects for galaxy-mass relations from the 6dF Galaxy Survey.

D. Burkey & A.N. Taylor

*Institute for Astronomy, University of Edinburgh, Royal Observatory, Blackford Hill, Edinburgh, U.K.
email:db@roe.ac.uk, ant@roe.ac.uk*

6 November 2018

ABSTRACT

We develop new methods to study the properties of galaxy redshift surveys and radial peculiar velocity surveys, both individually and combined. We derive the Fisher information matrix for redshift surveys, including redshift distortions and stochastic bias. We find exact results for estimating the marginalised accuracy of a two-parameter measurement of the amplitude of galaxy clustering, A_g , and the distortion parameter β . The Fisher matrix is also derived for a radial peculiar velocity survey and we discuss optimisation of these surveys for equal timescales. The Fisher Super-Matrix, combining both surveys, is derived. We apply these results to investigate the 6 degree Field Galaxy Survey (6dFGS), currently underway on the UK Schmidt Telescope (UKST). The survey will consist of $\sim 10^5$ K-band selected galaxies with redshifts and a subset of ~ 15000 galaxies with radial peculiar velocities. We find for the redshift survey that we can measure the three parameters A_g , Γ and β to about 3% accuracy, but will not be able to detect the baryon abundance, or the matter-galaxy correlation coefficient, r_g . The peculiar velocity survey will jointly measure the velocity amplitude A_v and Γ to around 25% accuracy. A conditional estimate of the amplitude A_v alone, can be made to 5%. When the surveys are combined however, the major degeneracy between β and r_g is lifted and we are able to measure A_g , Γ , β and r_g all to the 2% level, significantly improving on current estimates. Finally we consider scale dependence of r_g and the biasing parameter b . We find that measurements for these averaged over logarithmic passbands can be constrained to the level of a few percent.

Key words: Cosmology: theory – large-scale structure of Universe

1 INTRODUCTION

The quest to constrain cosmological parameters has been boosted in recent years by the emergence of large data sets from CMB experiments and galaxy surveys. In particular the first data release from WMAP combined with information from the 2 degree field (2dF) redshift survey and Lyman α forest data has allowed many cosmological parameters to be tightly constrained (Spergel et al. 2003). The Sloan Digital Sky Survey (SDSS) when complete, will constitute a fourfold increase in redshifts over 2dF. The 6 degree Field (6dF) galaxy survey (Wakamatsu, 2003, Colless, 1999) offers a unique combination of a wide field redshift survey with a homogeneous subset of peculiar velocities. It is the aim of this paper, in the context of the present data-boom, to predict the unique advantages of the 6dF galaxy survey over its contemporaries.

Galaxy surveys have long been an invaluable source of information in cosmology, allowing cosmologists to infer the large-scale clustering of matter in the Universe, and cosmo-

logical parameters. But despite their prominent role in our understanding of the clustering of matter, galaxy redshift surveys are fundamentally limited as a probe as we do not have a complete theory of galaxy formation from first principles. This limitation is characterised by the galaxy bias parameter, which is an unknown function relating the galaxy distribution to that of matter. In practice this function will be determined observationally, but its structure will help shape the theory of galaxy formation.

Galaxy redshift surveys also suffer from the well-known distortion due to the use of Doppler redshifts to infer distances. But redshifts are degenerate with peculiar velocities, the deviations from the Hubble flow generated by gravitational instability (Peebles, 1980). This projection of radial velocity information into redshift surveys provides additional complication to the analysis of the clustering pattern, but also injects extra information on the dynamics of large-scale structure which couples directly to the mass distribution.

In the local universe, the best way to probe the matter distribution is from the local peculiar velocity field. At

arXiv:astro-ph/0310912v1 31 Oct 2003

higher redshift gravitational lensing becomes the method of choice for probing the distribution of matter, while on even higher redshifts the CMB provides the only viable and accurate method.

By combining redshifts with distance indicators, such as the $D_n - \sigma$ relation, cosmologists have been able to estimate both true distance and radial peculiar velocities for local galaxies. Since estimating the true distance is a complicated, and time consuming process, these surveys have tended to be much smaller in size than the redshift surveys. In addition the distance estimators are subject to much larger uncertainties and biases than are the redshift estimates, and so have suffered from large uncertainties.

One of the problems with this programme has been the difficulty in collecting a large homogeneous sample. Progress in this field has been limited by the need to patch together a number of surveys with almost inevitable systematic differences. The subject of the different biases which plague peculiar velocity surveys is reviewed in Strauss and Willick (1995). There are two fundamental problems. $D_n - \sigma$ and Tully Fisher relations derived from different data will be systematically different, and a relation derived from one sample cannot be applied to another. Secondly, the observed quantities such as the velocity dispersions and apparent magnitudes needed for $D_n - \sigma$, will differ between surveys since each survey uses different observational methods and applies different corrections. The Mark III catalogue is one such compilation for which analysis has been done including the POTENT reconstruction where the 3-dimensional velocity is reconstructed from a potential - e.g. Kolatt et al. (2000). Another catalogue comprised of ~ 1600 field galaxies is the SFI catalogue. Both SFI and Mark III have been used to analyse the density power spectrum to constrain cosmological parameters as for example in Zehavi and Dekel (2000).

In the age of mega-surveys this problem of compiling inhomogeneous surveys should be alleviated by large coherent galaxy samples with accurate distance indicators. The 6dF Galaxy Survey is the first such data set. The 6dFGS is currently underway on the UK Schmidt Telescope (UKST). The survey will consist of $\sim 10^5$ K-band selected galaxies with redshifts and a subset of ~ 15000 of the brightest galaxies with radial peculiar velocities. The galaxies are sampled from the K-band 2 Micron All Sky Survey (2MASS) Extended Source Catalogue (Skrutskie, 2000) and so are dominated by early type galaxies. The advantage of the K-band is that it selects light from the old stellar population, and so presumably is a good indicator of the mass of the galaxy as a whole.

In addition to redshifts the 6dF will also collect galaxy distances. The 6dFGS will be the first combined redshift and velocity survey, with the advantage that the selection criteria for both surveys are matched. The prospect of a homogeneous and integrated galaxy redshift and radial velocity survey is a big step forward in the analysis of peculiar velocities, which have suffered from both sampling and inhomogeneity effects.

In this paper we develop an information-theory analysis of galaxy redshift surveys and radial peculiar velocity surveys, both individually and combined. Such an analysis is required both for survey design and to understand the sensitivity of the survey to cosmological parameters and so help

determine which parameters the survey can be optimised to measure. These methods are general to the construction and analysis of galaxy redshift and radial velocity surveys, and can readily be applied to, e.g., the Sloan Digital Sky Survey (SDSS) dataset or the radial velocity fields probed by galaxy clusters from Sunyaev-Zel'dovich surveys of the CMB, such as in the case of the Planck survey (Lawrence and Lange 1997).

The paper is laid out as follows. In Section 2 we describe our information theory methods, based on the Fisher information matrix. In Section 3 we derive the results we shall need for the analysis of galaxy redshift surveys while in Section 4 we apply these results to the problem of optimising their design. In Section 5 we estimate the sensitivity of a galaxy redshift survey to cosmological parameters, using the 6dF as our fiducial model. The analytic results we require for an analysis of the radial peculiar velocity field are derived in Section 6, and used to optimise such surveys in Section 7. Parameter estimation from a peculiar velocity survey is studied in Section 8, while in Section 9 we analyse the combined surveys. We present our conclusions in Section 10. There are also two appendices, with Appendix A deriving a series of useful formulae for the analysis of redshift surveys, and Appendix B calculating the bivariate Fisher matrix. We begin with a review of the Fisher information matrix.

2 FISHER INFORMATION ANALYSIS

2.1 The single field case

The Fisher information matrix measures the information content of a random field, $\phi(\mathbf{r})$, about a set of parameters, $\boldsymbol{\theta}$, that characterise that field. If this field is Gaussian distributed, the Fisher matrix is (Vogeley and Szalay 1996; Tegmark, Taylor and Heavens 1997, Tegmark 1997; Taylor and Watts 2001),

$$\mathcal{F}_{ij} = \frac{1}{2} \int \frac{d^3k}{(2\pi)^3} \partial_i \ln P_{\phi\phi}(\mathbf{k}) \partial_j \ln P_{\phi\phi}(\mathbf{k}) V_{\text{eff}}(\mathbf{k}) \quad (1)$$

where

$$\langle \phi(\mathbf{k}) \phi^*(\mathbf{k}') \rangle = (2\pi)^3 P_{\phi\phi}(k) \delta_D(\mathbf{k} - \mathbf{k}') \quad (2)$$

defines the power spectrum of a homogeneous field ϕ , and we have assumed $\langle \phi \rangle = 0$. The effective volume of the survey is

$$V_{\text{eff}}(\mathbf{k}) = \int_V d^3r \left(\frac{P_{\phi\phi}(\mathbf{k})}{P_{\phi\phi}(\mathbf{k}) + N(\mathbf{r})} \right)^2 \quad (3)$$

where the spatial integral is taken over the volume sampling the ϕ -field. As the field is Gaussian all the information characterising the field is contained in the power spectrum, $P_{\phi\phi}(\mathbf{k}) = P_{\phi\phi}(\mathbf{k}|\boldsymbol{\theta})$. The gradients in equation (1), $\partial_i \equiv \partial/\partial\theta_i$, are taken in parameter space.

If we randomly sample the field by a set of discrete points, the covariance of the sampled field is

$$C_{\phi\phi}(\mathbf{k}, \mathbf{r}) = [P_{\phi\phi}(\mathbf{k}) + N(\mathbf{r})] \quad (4)$$

where $N(\mathbf{r})$ is a noise term that may vary spatially.

The Fisher information matrix contains both the conditional error on a parameter on its diagonal and the marginalised error,

$$\langle \Delta\theta_i^2 \rangle_{\text{marg}} = [\mathcal{F}^{-1}]_{ii} \geq 1/\mathcal{F}_{ii}, \quad (5)$$

for the i^{th} parameter. The Cramér-Rao inequality (Kendall and Stuart 1969),

$$\langle \Delta\theta_i \Delta\theta_j \rangle \geq [\mathcal{F}^{-1}]_{ij} \quad (6)$$

where $\Delta\theta = \theta - \theta_0$ is the deviation of the parameters from their true value θ_0 , guarantees that the marginalised error is the smallest possible uncertainty on a parameter from a given measurement, and hence gives the minimum variance bound on marginalised parameter estimates. Furthermore the Cramér-Rao bound is an equality if maximum likelihood methods are applied.

If the parameter is the power itself the uncertainty on a measurement of the power, band averaged over a logarithmic passband of width $d \ln k$, is given by (Feldman, Kaiser and Peacock 1994)

$$\Delta P(k) = \frac{2\pi P(k)}{\sqrt{k^3 d \ln k V_{\text{eff}}(k)}}. \quad (7)$$

2.2 Multiple Fields

Multiple fields can be incorporated into the Fisher Matrix formalism by generalising the definition of the data vector and its covariance matrix. Assuming we have two fields, ϕ_1 and ϕ_2 , we can form a covariance super-matrix

$$C = \begin{pmatrix} C_{11} & C_{12} \\ C_{21} & C_{22} \end{pmatrix} \quad (8)$$

where each of the individual covariances $C_{\alpha\beta} = \langle \phi_\alpha \phi_\beta \rangle$ where $\alpha, \beta = 1, 2$ labels the fields. This super-matrix can be used to generate a Fisher super-matrix (eg Zaldarriaga, Spergel and Seljak 1997, Bouchet, Prunet and Sethi 1999),

$$\mathcal{F}_{ij} = \int d^3k d^3r \sum_{XY} \partial_i C_X [\text{Cov}(C_X C_Y)]^{-1} \partial_j C_Y. \quad (9)$$

The full expression of the Fisher super-matrix is given in the Appendix by equation (66).

2.3 Parameter correlation coefficient

As well as the uncertainty on a measurement of a parameter set from a given survey, the Fisher matrix can also be used to estimate the correlations between measured parameters. The parameter correlation coefficient,

$$\gamma_{ij} = \frac{\langle \Delta\theta_i \Delta\theta_j \rangle}{\Delta\theta_i \Delta\theta_j} = \frac{F_{ij}^{-1}}{\sqrt{F_{ii}^{-1} F_{jj}^{-1}}}, \quad (10)$$

shows the degree of degeneracy between two parameters and allows one to identify the largest eigenvalue of the parameter covariance matrix. This is of much use, as the degeneracy between parameters can be the major limiting factor in parameter estimation. Knowing the principle degeneracy in parameter space, one can choose to increase the set of modes, preferentially adding information so as to decrease this degeneracy using the GOMA data compression analysis discussed in Taylor et al. (2001).

3 COSMOLOGICAL RANDOM FIELDS

The design of galaxy redshift surveys has been investigated before by Heavens and Taylor (1997) who discussed the optimisation problem, and by Tegmark (1997) who calculated the uncertainty on parameters in linear theory, ignoring the effect on redshift-space distortions. Taylor and Watts (2001) generalised this to the nonlinear regime, and included both redshift distortions and nonlinear bias. Here we summarise these results for the linear analysis, assuming a general stochastic biasing model (Dekel and Lahav 1999) to relate the matter density field to the galaxy field.

3.1 Galaxy density and radial velocity fields

We shall assume for our analysis that the relevant field is the linear galaxy redshift-space density perturbation in the plane-parallel approximation. We write

$$\delta_g^s(\mathbf{k}) = D(k\sigma_v\mu)[(b_L + \mu^2 f)\delta_m(\mathbf{k}) + \epsilon] \quad (11)$$

where $f \equiv d \ln \delta / d \ln a \approx \Omega_m^{0.6}$ (Peebles 1980) is the growth index of density perturbations, b_L is a linear bias parameter, $\delta_m(\mathbf{k})$ is the linear matter density field, $\mu = \hat{\mathbf{r}} \cdot \hat{\mathbf{k}}$ is the cosine angle between the wave-vectors of the density field and the observers line of sight and ϵ is a stochastic bias term. We assume $\langle \epsilon \rangle = 0$ and $\langle \epsilon^2 \rangle = \sigma_\epsilon^2$. We have also included a nonlinear redshift distortion term

$$D(k\sigma_v\mu) = (1 + k^2 \sigma_v^2 \mu^2 / 2)^{-1/2} \quad (12)$$

where σ_v is the pairwise radial velocity dispersion.

We define a second bias parameter as the ratio of power in the galaxy distribution $P_{gg}(k)$, to that in the matter fields, $P_{mm}(k)$:

$$b = \frac{P_{gg}(k)}{P_{mm}(k)} = b_L^2 + \frac{\sigma_\epsilon^2}{P_{mm}(k)}. \quad (13)$$

We may also introduce a galaxy correlation coefficient, r_g , defined by

$$r_g = \frac{P_{gm}(k)}{\sqrt{P_{gg}(k)P_{mm}(k)}} = \frac{b_L}{b} \quad (14)$$

(Dekel and Lahav 1999) which will allow us to change between the two bias parameters. Although b_L is more physical, it is b which is more commonly measured.

We choose our second field to be the radial gradient of the radial peculiar velocity field, defined in Fourier space as

$$u'(\mathbf{k}) = \frac{\partial}{\partial \mathbf{r}} \hat{\mathbf{r}} \cdot \mathbf{v}(\mathbf{k}) = -\mu H f(\Omega_m) \delta_m(\mathbf{k}) \quad (15)$$

where H is the Hubble parameter. The modes of the radial velocity are uncorrelated with the modes of the density field. However the Fourier space radial gradient of the radial velocity *is* correlated and will yield a cross power spectrum.

The auto- and cross-power spectra of these two fields are

$$P_{gg}^s(\mathbf{k}) = D^2(k\sigma_v\mu)(1 + 2\mu^2 r_g \beta + \mu^4 \beta^2) b^2 P_{mm}(k) \quad (16)$$

$$P_{u'u'}(\mathbf{k}) = \mu^4 H^2 \beta^2 b^2 P_{mm}(k), \quad (17)$$

$$P_{gu'}^s(\mathbf{k}) = -\mu^2 H \beta D(k\sigma_v\mu)(r_g + \mu^2 \beta) b^2 P_{mm}(k), \quad (18)$$

where

$$\beta \equiv \frac{f(\Omega_m)}{b} \quad (19)$$

is the linear redshift distortion parameter.

The three spectra to be measured are the redshift-space galaxy power spectrum, $P_{gg}^s(\mathbf{k})$, the radial velocity gradient power spectra, $P_{u'u'}(\mathbf{k})$, and the cross-spectra of these fields, $P_{gu'}^s(\mathbf{k})$.

The noise terms associated with these fields are

$$N_{gg}(r) = \frac{1}{n_g(r)}, \quad (20)$$

$$N_{u'u'}(r) = \mu^2 k^2 \frac{\sigma_{DI}^2(r)}{n_v(r)}, \quad (21)$$

$$N_{gu'}(r) = 0, \quad (22)$$

where $n_g(r)$ and $n_v(r)$ are the number densities of the galaxy and velocity surveys, respectively. The factors of μ^2 and k^2 are due to our use of the radial velocity gradient. We quantify the number densities in Sections 4 and 7. The noise term for radial velocities arises from the intrinsic uncertainty on galaxy positions due to the dispersion in the D_n - σ relation for ellipticals. This can be approximated by

$$\sigma_{DI}(r) = \sigma_0 H r e^{r/r_{\text{err}}}, \quad (23)$$

where σ_0 is the fractional error on the distance indicator. We allow the fractional distance error to blow up beyond some fiducial distance, r_{err} . We choose a conservative r_{err} of $135 h^{-1} \text{Mpc}$ (which is 90 % of the 6dF median depth), but allowing this to decrease to as low as 50% of the median depth had little effect on our results.

3.2 The matter power spectrum and cosmological parameters

Throughout we define the matter power spectrum by

$$P_{mm}(k) = Q^2 k^n T^2(k; \Gamma, \omega_b), \quad (24)$$

where Q is the amplitude of matter perturbations, n is the primordial spectral index of perturbations and $T(k)$ is the matter transfer function. The dependent parameters of the transfer function are the so-called ‘‘shape parameter’’,

$$\Gamma = \Omega_m h \quad (25)$$

which stretches the scale of the transfer function, and

$$\omega_b = \Omega_b h, \quad (26)$$

where Ω_b is the density parameter of baryonic matter. Here we use the form of the transfer function given by Eisenstein and Hu (1998).

The other parameters which will be of interest to us are the amplitude of galaxy clustering and the amplitude of the velocity field. As we shall assume linear theory throughout, these are respectively

$$A_g = bQ \quad (27)$$

where b is the linear galaxy bias parameter, and

$$A_v = f(\Omega_m)Q. \quad (28)$$

Also of interest is the mass-galaxy correlation coefficient r_g , and as we shall assume the galaxy survey is in redshift-space, the final parameter is the redshift-space distortion parameter, β .

For the purposes of this paper we shall assume the primordial spectrum is scale-invariant so that $n = 1$.

Hence the parameters we shall investigate are the six non-degenerate parameter set $(A_g, A_v, \Gamma, \omega_b, \beta, r_g)$. The model we shall use has fiducial values of $(Q, h, \Omega_m, \omega_b, b, r_g) = (5 \times 10^{-5}, 0.65, 0.3, 0.025, 1, 1)$ giving the measurable parameters the values $(A_g, A_v, \Gamma, \omega_b, \beta, r_g) = (5 \times 10^{-5}, 0.486 \times 5 \times 10^{-5}, 0.195, 0.025, 0.486, 1)$.

4 THE GALAXY REDSHIFT SURVEY

4.1 Survey parameters

A galaxy redshift survey can be parameterised by the fractional sky coverage, f_{sky} , and the mean radial density of galaxies in the sample, which we parameterise by

$$n_g(r) = N_g \frac{a}{r_*^3 \Gamma [3/a]} e^{-(r/r_*)^a} \quad (29)$$

where r_* is a convenient survey depth scale, N_g is the total number of galaxies and typically $a = 1.5$.

Rather than use r_* we use the median depth of the survey ($r_m \approx 1.5r_*$) and the number of galaxies available in the survey roughly scales as

$$N_g \approx 4. \times 10^{-2} \alpha r_m^{3.125}, \quad (30)$$

from fitting the near infrared differential number counts compiled in Kochanek et al. (2000).

The sampling fraction, α , is simply the fraction of sources expected at any redshift which are actually observed. We shall assume that space is Euclidean. The three survey parameters are then f_{sky} , r_m and α .

4.2 Optimisation of a Galaxy Redshift Survey

The problem of optimisation of a galaxy redshift survey has been previously considered by Heavens and Taylor (1997), who showed that the optimisation for a fixed timescale reduces to a one-parameter optimisation problem. We first need to choose a parameter for which to optimise. Here we choose the amplitude of galaxy perturbations, A_g , where the conditional error on a measurement is given by

$$\frac{\Delta A_g}{A_g} = \left[\frac{1}{2} \int \frac{d^3 k}{(2\pi)^3} V_{\text{eff}}^g(k, \mu) \right]^{-1/2}. \quad (31)$$

We now assume the timescale for the redshift survey is a constant and scales as

$$t = t_0 \alpha f_{\text{sky}} (r_m / h^{-1} \text{Mpc})^7, \quad (32)$$

where t_0 is some fixed timescale. We take as our baseline a 2 year survey where $t/t_0 \approx 7 \times 10^{17}$. The strongest constraint then comes from the survey depth. The uncertainty on parameters scales as $\Delta\theta \propto f_{\text{sky}}^{-1/2}$, while the time scales as $t \propto f_{\text{sky}}$, indicating, as is well known, that as large a solid angle as possible should be chosen. With this time constraint the survey median depth is

$$r_m = 150 (\alpha f_{\text{sky}})^{-1/7} h^{-1} \text{Mpc}. \quad (33)$$

This states that the depth of the survey is increased at the expense of sparse sampling or reduced sky coverage. We can now minimise the uncertainty on A_g .

Figure 1 shows the results of minimising the fractional error on the galaxy clustering amplitude as a function of

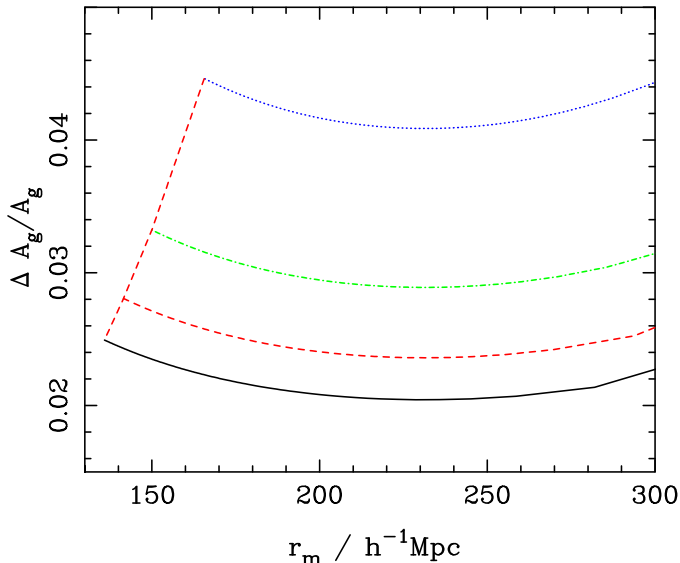


Figure 1. Optimisation of the 6dF redshift survey. Here we plot the fractional error on a conditional measurement of the amplitude of galaxy clustering, A_g , as a function of survey median depth, r_m . The lines are for constant survey timescales with sky coverage of unity (bottom), three quarters (second from bottom), a hemisphere (third from bottom) and a quarter (top).

survey depth, for a fixed timescale. Each of the lines is for a different sky coverage. The approximate relation we use between limiting K band magnitude and median depth is

$$K_{limit} \approx 5 \log \left(\frac{r_m}{h^{-1} \text{Mpc}} \right) + 1.865. \quad (34)$$

The sampling fraction for each value of r_m may be calculated from equation (33). The dashed line in Figure 1 shows the physical limit $\alpha = 1$. The optimal survey is a shallow all-sky survey with depth $r_m = 140 h^{-1} \text{Mpc}$. For a hemisphere this increases slightly to $r_m = 150 h^{-1} \text{Mpc}$, while the optimal value of $\alpha \approx 0.7$ is fairly insensitive to either f_{sky} or r_m . The increase in the uncertainty in the fractional error in A_g with increased depth is due to the decrease in the total number of galaxies in the survey. At the extreme of very large r the fractional uncertainty in A_g tends towards $A_g \sim r^{6.5}$.

Figure 2 shows the linear galaxy power spectrum using the optimal redshift survey parameters for the 6dF, along with the expected conditional error bars in band averaged pass-bands of width $\Delta \ln k = 0.5$. We have also plotted the effective volume, $V_{\text{eff}}^g(k)$, which indicates where the information is maximised in the survey. Finally we have also plotted the noise per mode, $k^3/2\pi^2\bar{n}$, where \bar{n} is the average density of the survey. For the rest of the analysis we use $K_{limit} = 12$, $f_{sky} = 0.5$, $r_m = 150 h^{-1} \text{Mpc}$ and $\alpha = 0.7$.

5 PARAMETER FORECASTS FOR THE 6dF REDSHIFT SURVEY

In linear theory a galaxy redshift survey based on a CDM model contains three free parameters: the amplitude of the galaxy power spectrum, $A_g = bQ$, the scale of the break,

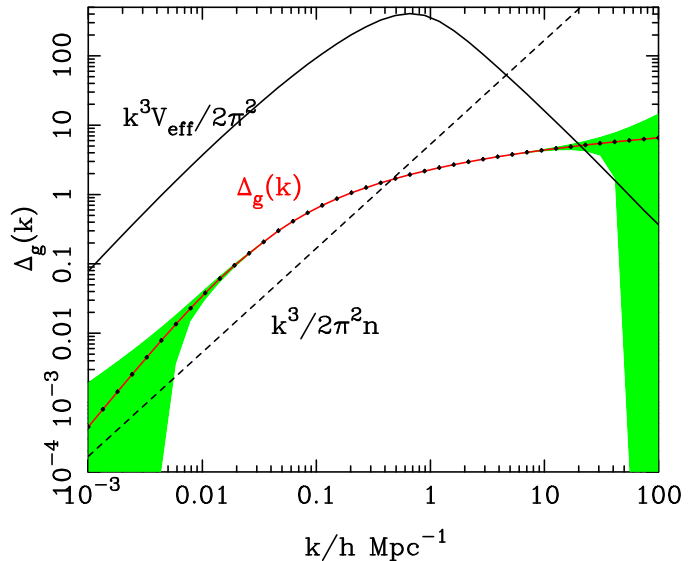


Figure 2. The linear galaxy power spectrum with fiducial LCDM parameters (solid light line). Also plotted are the expected band averaged error on measured power pass-bands (grey area), and the effective survey volume $V_{\text{eff}}^g(k)$ (dark solid line) and the shot-noise per mode (dashed line), for the 6dF redshift survey. We parameterise the 6dF survey by its sky coverage, depth and total number of galaxies.

parameterised by $\Gamma = \Omega_m h$ and the redshift distortion parameter, $\beta = \Omega^{0.6}/b$. Other parameters that could be considered are the small-scale pairwise velocity dispersion, σ_v , or the baryonic density parameter, Ω_b , which can introduce oscillations in the the matter power spectrum. Other possible parameters include the spectral index n (Tegmark 1997) or the correlation between luminous and dark matter r_g . We consider the estimation of five parameters A_g , Γ , β , Ω_b and r_g .

5.1 The information content of the redshift-space galaxy power spectrum

The information content of a galaxy redshift power spectrum can be examined per Fourier mode by plotting the derivatives of the log-power with respect to the parameters, $d \ln P_{gg}^s(k)/d\theta$. In geometric terms this derivative can be thought of as a vector in Hilbert space, and the Fisher matrix as the dot product of such vectors. Hence the more similar two curves are, the more “parallel” they are and so the greater the degeneracy between the parameters. In the extreme that two curves are identical the Fisher matrix becomes singular and the uncertainty becomes infinite.

Figure 3 shows that the derivatives for the five parameters we can extract from linear theory, $\theta = (A_g, \Gamma, \beta, \omega_b, r_g)$. The A_g -derivative is a constant across all modes, as expected. Similarly both r_g and β are almost constants, as they appear in the normalisation of the galaxy power spectrum. Hence we can expect some degeneracy between these three parameters.

The final two parameter derivatives, Γ and ω_b are also similar. This is because Γ parameterises the break in the

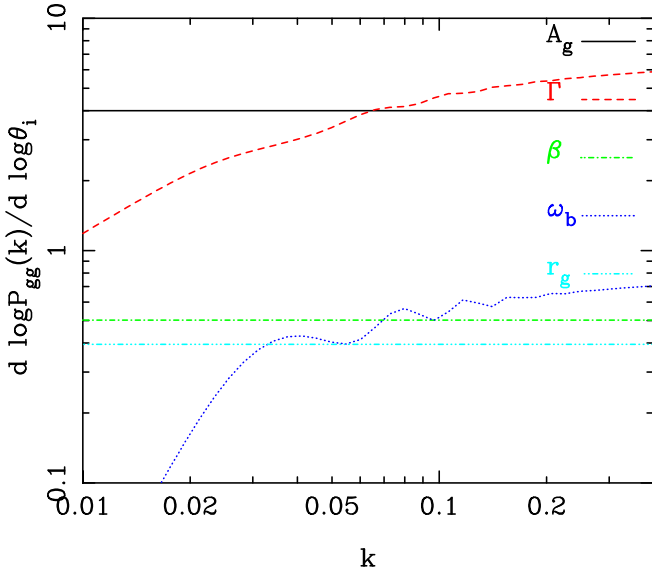


Figure 3. Derivatives of the matter power spectrum

CDM power spectrum, between retarded modes inside the horizon at matter-radiation equality and growing modes outside, while ω_b parameterises the effect of baryonic damping of perturbations inside the horizon when the baryonic fluid is oscillating. Hence both parameters are related to two physically different effects that produce similar damping of the matter power spectra. An effective shape parameter can be defined by (Peacock and Dodds 1994)

$$\Gamma_{\text{eff}} = \Gamma e^{-2\Omega_b h} \quad (35)$$

which crudely models both effects but explicitly shows the degeneracy. On scales larger than the break, the effects of the baryons dies away quicker, and so on the largest scales the power spectra contains more information on Γ than on ω_b .

5.2 The amplitude of galaxy clustering and redshift distortion parameter

In the limit of negligible shot noise, it is possible to calculate analytically the two-parameter Fisher matrix for A_g and β . The details of this are shown in Appendix A. From equation (54) the correlation coefficient between the two parameters is $\gamma_{A_g\beta} = -0.78$, which is very close the value found by Taylor et al (2001) for the Point Source Redshift Survey (PSCz). The strong anti-correlation is due to the similar effects of the parameters on the power spectrum, as they both appear in the amplitude of the redshift-space power. From equation (52) we can read off the fractional errors: $\Delta A_g/A_g = 0.01$, and $\Delta\beta/\beta = 0.057$ for current typical survey sizes at the limit of linear theory $k \approx 0.2 h \text{Mpc}^{-1}$.

For a single parameter estimate of β , again in the absence of shot noise we find;

$$\frac{\Delta\beta}{\beta} = \sqrt{\frac{2\pi^2}{Vk^3}} \left(2 + \frac{1}{1+\beta} - \frac{3 \tan^{-1}(\sqrt{\beta})}{\sqrt{\beta}} \right)^{-1/2}, \quad (36)$$

where V is the survey volume, and k is the maximum

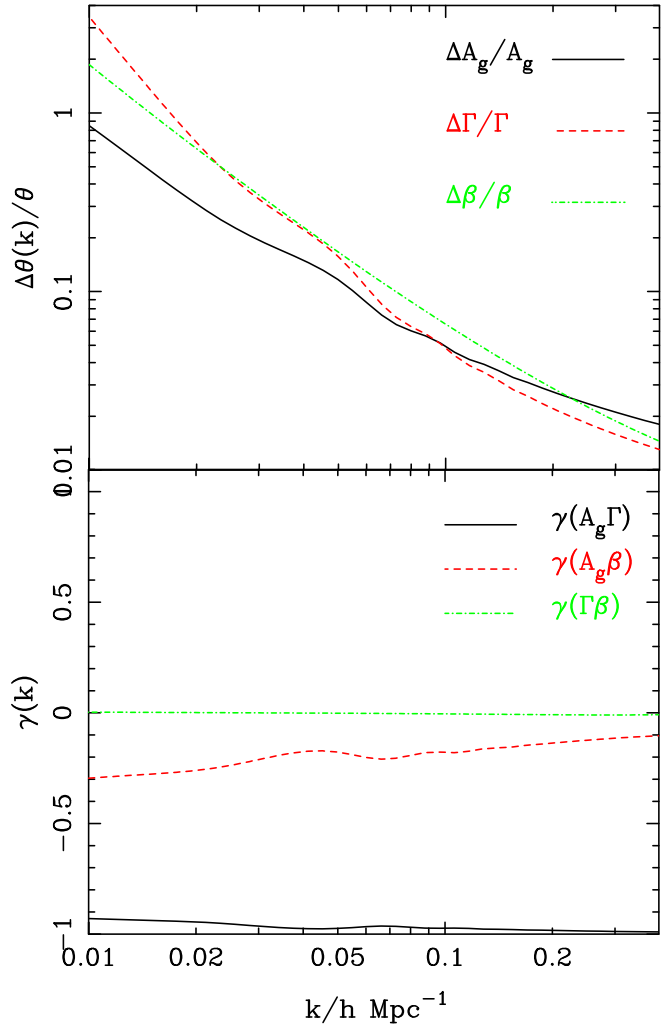


Figure 4. Upper plot: The expected fractional uncertainty on A_g , Γ and β from the 6dF redshift survey. **Lower plot:** The correlations between A_g , Γ and β . We model the survey as described in the text.

wavenumber used to estimate β . For $\beta = 0.5$, and $k = 0.2 h^{-1} \text{Mpc}$ this gives a fractional uncertainty of

$$\frac{\Delta\beta}{\beta} = \left(\frac{V}{4.5 \times 10^4 [h^{-1} \text{Mpc}]^3} \right)^{-1/2}. \quad (37)$$

Hence, even for a well-sampled galaxy redshift survey, the effective volume has to be large to beat down the sampling noise on a determination of β . To achieve a 1% error, assuming all other parameters are known, requires a survey with volume $V \approx 4.5 \times 10^8 [h^{-1} \text{Mpc}]^3$, over four times larger than the 2dF, 6dF or SDSS redshift surveys. Hence to achieve high accuracy on cosmological parameters in the linear regime requires an order of magnitude increase in survey size. However even for these surveys, with volumes of order $V \approx 10^8 [h^{-1} \text{Mpc}]^3$, we can expect an accuracy of $\Delta\beta/\beta \approx 0.02$. An alternative to going large is to extend the analysis into the nonlinear regime, as outlined by Taylor & Watts (2001). Finally, the uncertainty can be reduced by combining data sets, as investigated here.

5.3 Three parameter set: A_g , Γ and β

Introducing extra correlated parameters into the analysis causes uncertainties to increase, and adds extra complexity to the analysis. Hence we first consider a reduced 3-parameter set consisting of A_g , Γ and β , and then see how adding new parameters changes our results.

Figure 4 shows the expected fractional marginalised uncertainties from the 6dF redshift survey plotted as a function of maximum wavenumber analyzed. The scale of interest for linear analysis is around $k \approx 0.2 \text{ hMpc}^{-1}$. At this wavelength the best estimated parameter is Γ which is constrained to within about 2%. The uncertainty on A_g and β is about 3%. For β this is close to our conditional estimate in Section 5.2.

Figure 4 also shows the correlation coefficient for these parameters. The strongest correlation is between the amplitude of galaxy clustering, A_g , and the shape parameter, Γ , with $\gamma(A_g\Gamma) \approx -0.95$. This arises because a change in amplitude can be mimicked by a shift in scale. The least correlated parameters are Γ and β .

Intermediate is the correlation between A_g and β . This is of particular interest as their combination gives (Taylor et al 2001)

$$A_g\beta = Qf(\Omega_m) \approx Q\Omega_m^{0.6}, \quad (38)$$

and so provides an independent estimate of the amplitude of matter perturbations. The correlation of these parameters can be calculated in the limit of negligible shot-noise, and ignoring other parameters is given by equation (54) in Appendix A. For $\beta = 0.5$ we find $\gamma_{A_g\beta} = -0.78$, very close to the value we find for a two parameter analysis.

As these parameters are anti-correlated, the combination $A_g\beta$ has a smaller formal error than either A_g or β . This arises because the combination $A_g\beta$ marginalises over the A_g - β parameter space along the longest line of the degeneracy, so that the marginalised combination has a smaller error than its components. This effect is shown later, in Section 9 figure 11.

5.4 Four parameter set: A_g , Γ , β and ω_b

Introducing a fourth parameter, ω_b , has little effect on the uncertainties on A_g and β on scales $k > 0.05 \text{ hMpc}^{-1}$, as shown in Figure 5. Figure 5 shows that this is due to the weak correlation between ω_b and these parameters. However the strong correlation between ω_b and Γ , $\gamma(\Gamma\omega_b) \approx 0.9$, which we expect from our discussion in Section 5.1, degrades the uncertainty on Γ . Disappointingly the uncertainty on a measurement of ω_b is large, $\Delta\omega_b/\omega_b \approx 0.45$, which reflects its weak effect on the matter power spectrum. As with all the parameters, the main way to improve on sensitivity is with a larger redshift survey.

Since ω_b and Γ are correlated would we do any better by estimating the baryon fraction,

$$f_b = \frac{\omega_b}{\Gamma} = \frac{\Omega_b}{\Omega_m}, \quad (39)$$

rather than simply ω_b ? Unfortunately not. Although these parameters are positively correlated, and so the marginalised combination will project out along the longest axis of the ω_b - Γ error ellipse, making the fractional error on f_b smaller, other correlations, particularly between ω_b and A_g , prevent

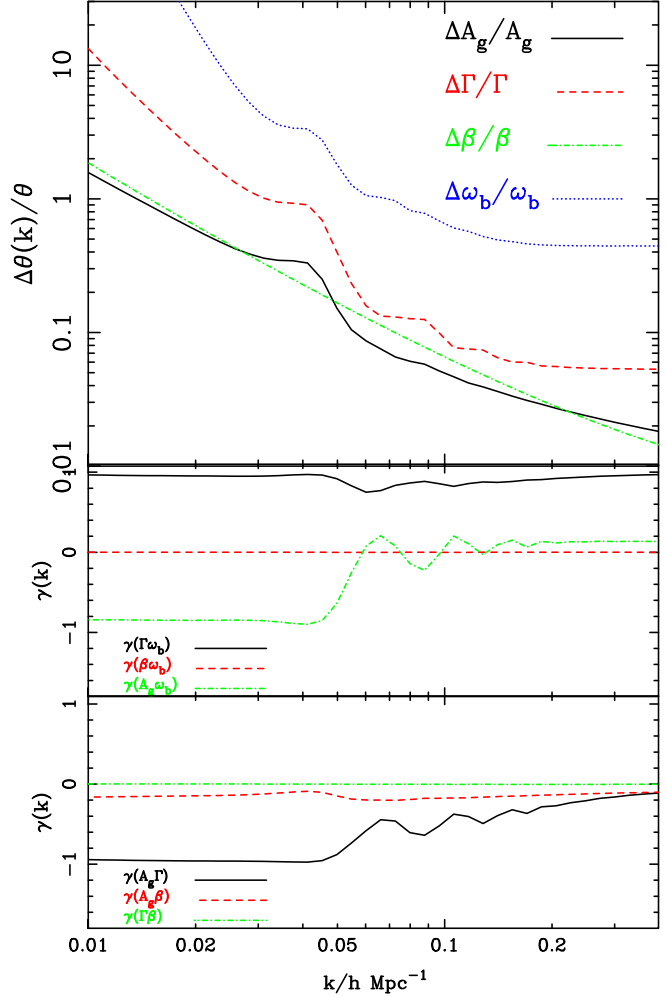


Figure 5. Upper plot: Predicted errors for a four parameter analysis involving ω_b . **Lower plot:** Correlations in a four parameter space with ω_b

any improvement. We have re-analysed the survey with f_b replacing ω_b throughout and find negligible change in our results. We conclude that the main limiting factor here is the survey volume.

In order to reduce the error on ω_b to the 10% level we predict one would require a survey some 10 times larger.

5.5 Four parameter set: A_g , Γ , β and r_g

Instead of ω_b , we could have chosen r_g as our fourth parameter. Figure 6 shows that this time A_g and Γ are unaffected by this new parameter, but the uncertainty on β is dramatically increased, with both the fractional errors on β and r_g around 35%. Again this can be traced to the expected degeneracy between r_g and β discussed in Section 5.1, and shown in Figure 6, where $\gamma_{\beta r_g} \approx -1$. Interestingly the correlation between A_g and β has now become positive, so that the error on their combination will be increased.

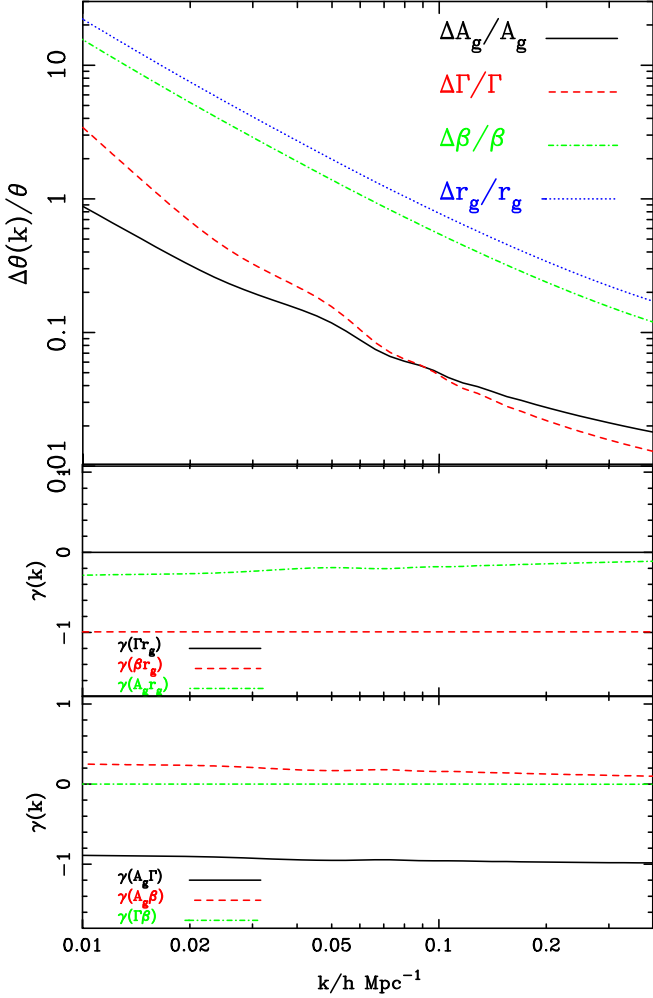


Figure 6. Lower plot: Uncertainties for a four parameter analysis involving r_g . **Lower plot:** The correlations between A_g , Γ , β and r_g

6 GALAXY VELOCITY SURVEY

The application of Fisher information methods to galaxy velocity surveys has so far been limited. Here we derived for the first time the Fisher matrix from parameters from such a radial velocity survey, and use it to find the optimal survey parameters, estimate the conditional errors on a measurement of the velocity power spectrum and estimate the marginalised errors on cosmological parameters. In Section 9 we combine the radial velocity and galaxy redshift surveys.

Figure 7 shows the 3-D velocity power spectrum for our fiducial LCDM cosmology, and the effective survey volume, $k^3 V_{\text{eff}}^v(k)/2\pi^2$, for a model 6dF velocity survey.

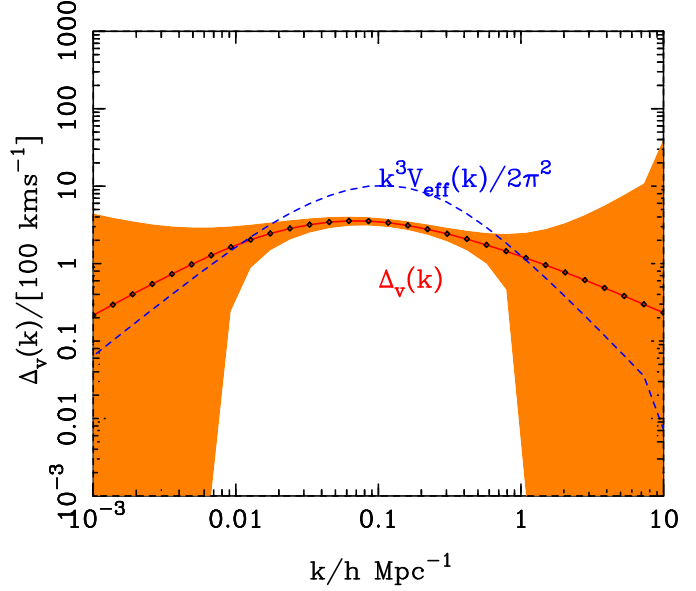


Figure 7. The peculiar velocity power spectrum, $\Delta_v(k) = \sqrt{k^3 P_v(k)}/2\pi^2$ with predicted noise and effective volume for the 6dF peculiar velocity survey. The velocity survey is parameterised by f_{sky} , cut-off depth, α_v and the accuracy of the distance indicator.

7 VELOCITY SURVEY OPTIMISATION

7.1 Velocity survey parameters

The velocity survey can be parameterised by the fractional sky coverage, f_{sky} and the mean radial density of galaxies in the sample, which is parameterised as for the galaxies (equation 29). The early type galaxies for the velocity survey will be a subset of this group and so for analysis of the velocity survey the number count needs to be multiplied by a factor of 0.3 and the analysis limited to r_m which is the cut-off in the 6dF velocity survey. We shall again assume a Euclidean universe for simplicity, and as we are working at low redshift. The survey can then be parameterised by f_{sky} , r_m , α_v and σ_0 , the expected fractional error in the distance indicator.

The angular part of the effective volume for the velocity survey can be integrated analytically and yields

$$V_{\text{eff}}^u(k) = 2\pi f_{\text{sky}} \int_0^\infty dr r^2 \Theta \left[\frac{n_u(r) P_{uu}(k)}{\sigma_{DI}^2(r)} \right] \quad (40)$$

where the function $\Theta(z)$ is defined in Appendix A, equation (50). Figure 7 shows the dimensionless effective survey area. The peak of the effective volume again indicates where the information content is maximised.

7.2 Band-averaged power

As well as showing the effective volume Figure 7 shows the error bars expected for a measurement of band-averaged velocity power in a series of pass-bands, using equation (7). The power spectrum plotted is the three dimensional velocity power spectrum but the error bars reflect the fact that this will be derived using only radial velocity data. The pass bands are of width $\Delta \ln k = 0.5$ and so this plot may

be directly compared with the corresponding band averaged power for the redshift survey in Figure 2. The velocity power spectrum has much larger error bars which is a reflection of the smaller size of the velocity data set.

7.3 Optimisation of a velocity survey

As with the redshift survey we wish to know whether the velocity survey can be optimised in the sense of maximising the information content for the minimum observing time. To optimise the survey, we choose the amplitude of the power spectrum as a fiducial optimisation parameter, where

$$\frac{\Delta A_v}{A_v} = \left[\int \frac{d \ln k}{4\pi^2} k^3 V_{\text{eff}}^v(k) \right]^{-1/2}, \quad (41)$$

and we consider the case of equal-time surveys.

The timescale for a velocity survey scales as the total number of sources in the survey, $N \sim r^3$, the reciprocal of the effective flux of the sources, $S \sim r^{-2}$, the distance error per source, σ_{DI} , the fraction of the sky surveyed, f_{sky} , and the fraction of the sources sampled, α . The timescale for a velocity survey then scales as

$$t \approx \alpha_v f_{\text{sky}} \left(\frac{\sigma_0}{\text{kms}^{-1}} \right)^{-2} \left(\frac{r_m}{h^{-1}\text{Mpc}} \right)^7 t_0 \quad (42)$$

where t_0 is a constant timescale. For a survey of a few years we find the ratio $t/t_0 \approx 2 \times 10^{13}$.

We can now minimise the fractional uncertainty on the amplitude of the velocity power spectrum, A_v , in survey-space with the equal-time constraint and the restrictions $f_{\text{sky}}, \alpha_v \leq 1$. In our model, the overall uncertainty on parameters scales as $\Delta\theta \propto f_{\text{sky}}^{-1/2}$, so all our results and timescales can be scaled by the fraction of sky surveyed. In the following analysis we fix the value of f_{sky} and optimise in terms of the remaining survey parameters. In addition the uncertainty in source distance per source, σ_0 , and the source sampling rate, α_v , always appear in the ratio σ_0^2/α_v , further reducing the number of free survey parameters we need to consider. Finally, we can relate the remaining parameter, r_m to the other parameters by

$$r_m \approx 150 \left[\frac{1}{\alpha_v f_{\text{sky}}} \left(\frac{\sigma_0}{\text{kms}^{-1}} \right)^2 \right]^{1/7} h^{-1}\text{Mpc}. \quad (43)$$

Hence we only need to optimise the survey with respect to the degenerate parameter

$$\nu = \frac{1}{\sqrt{\alpha_v}} \left(\frac{\sigma_0}{\text{kms}^{-1}} \right). \quad (44)$$

In practice there is a lower limit to the accuracy of the distance indicator. The current best accuracies from the D_n - σ relation provide distance estimates with a minimum scatter of $\sigma_{\text{min}} \approx 0.1 \text{kms}^{-1}$ e.g. (Jorgensen et al. 1993; Gregg 1995), and so we shall optimise the survey design in terms of the new parameter

$$\eta = \frac{1}{\sqrt{\alpha_v}} \left(\frac{\sigma_0 + \sigma_{\text{min}}}{\text{kms}^{-1}} \right) \quad (45)$$

which better reflects the survey's limitations.

Figure 8 shows the fractional uncertainty on a conditional measurement of A_v for equal-time surveys as a function of η and where the different curves correspond to different sky fractions, f_{sky} . The lowest, solid line is for an all-sky

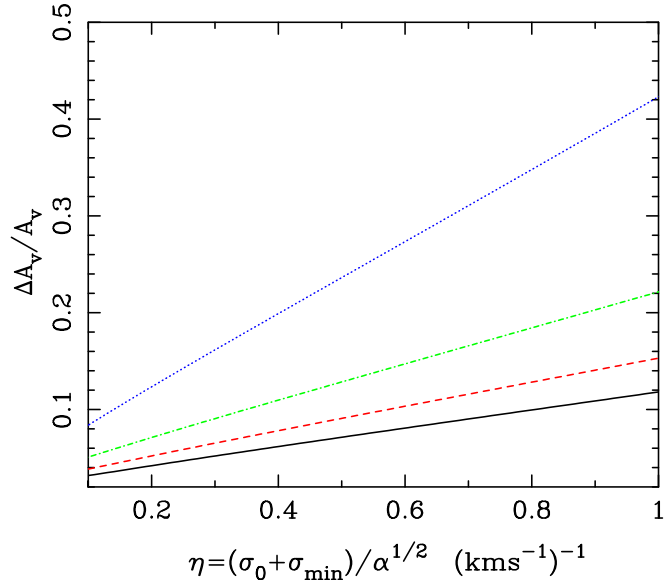


Figure 8. The normalised fractional uncertainty on the amplitude of the velocity power spectrum for the degenerate parameter $\eta = \frac{(\sigma_0 + \sigma_{\text{min}})}{\text{kms}^{-1}} \frac{1}{\sqrt{\alpha_v}}$, for equal-time surveys. The four lines correspond to different sky fractions (see Figure 1).

survey, with higher lines reduced by one quarter. The expected 6dF velocity survey lies somewhere between the top two lines depending on dust extinction from the plane of the galaxy.

The other parameter that this analysis will depend on is the upper wavenumber used in the analysis, k_{max} . Linear theory is reasonably robust up to $k = 0.2 h^{-1}\text{Mpc}$. In practice it was found that the optimal survey parameters changed little with changes in k_{max} , so that our results with $k_{\text{max}} = 0.2 h\text{Mpc}^{-1}$ are quite general.

Our results show that the optimal strategy is to be as accurate as possible in the distance determinations at the expense of going deep. In fact the absolute optimal strategy is found to be impossible with current distance indicator limits – if the distances could be better constrained then we could do even better. The reason for this is that by $k \approx 0.2 h\text{Mpc}^{-1}$ the power spectrum is already becoming dominated by shot noise. If there were more sources (and so less shot noise) this would have the same effect as increasing α in the degenerate parameter η and so the optimal value for σ_0 would also increase. The bottom line is that the survey should be as well sampled and as accurate as possible before going deep.

For the rest of this analysis we assume $\sigma = 0.1 \text{kms}^{-1}$, $\alpha_v = 0.2$, $f_{\text{sky}} = 0.5$ and $\eta = 0.2$.

8 COSMOLOGICAL PARAMETER FORECASTS FROM VELOCITY SURVEYS

In the linear regime the properties of the velocity field can be specified by just two parameters – the amplitude of the velocity power spectrum, A_v , and the shape parameter, Γ . Figure 9 shows the fractional error expected on A_v and Γ for an optimal survey, as a function of maximum wavenumber

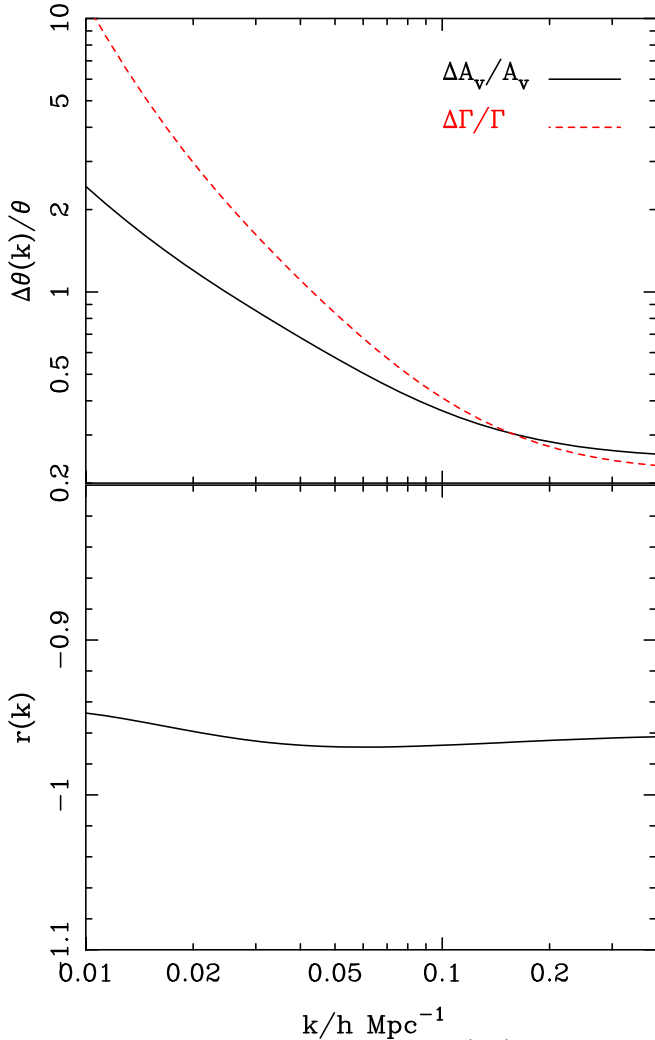


Figure 9. The expected fractional error (top) and correlation coefficient (bottom) for the amplitude and shape parameter of the 6dF velocity power spectrum. The survey parameters are discussed in the text.

analyzed. If we truncate the analysis at $k = 0.2 h^{-1} \text{Mpc}$, the fractional uncertainty in both A_v and Γ is expected to be $\approx 25\%$, ignoring any systematic uncertainties.

Figure 9 also shows the parameter covariance coefficient

$$\gamma_{A_v \Gamma}(k) = \frac{\langle \Delta A_v \Delta \Gamma \rangle}{\Delta A_v \Delta \Gamma} \approx -0.8 \quad (46)$$

as a function of wavenumber. It is because of this anticorrelation that a joint constraint of A_v and Γ is difficult. If we assume a value for Γ obtained from the redshift survey, Figure 8 shows that A_v may be constrained on its own to $\approx 5\%$.

9 COMBINING DATA SETS

In this section we combine the information content of the radial velocity field and the galaxy redshift survey. We calculate the Fisher matrix using equation (9) which is written explicitly in Appendix B. As explained in Section 3 we now

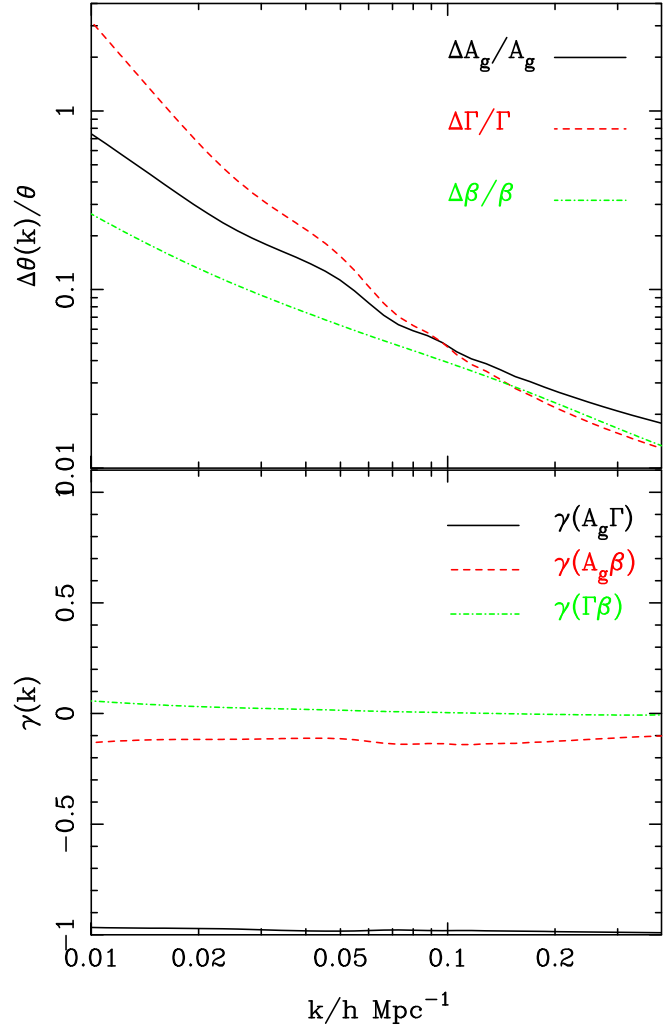


Figure 10. Supermatrix fractional errors and correlations between A_g , Γ and β . These predictions are for a combination of the 6dF redshift and peculiar velocity surveys.

work with the radial velocity gradient as this will yield a cross-power spectrum with the density field.

9.1 Three parameter set

To see how combining redshift and velocity data affects parameter estimation we begin with our three parameter set; A_g , Γ and β . Figure 10 shows the uncertainties and correlations of this set. Comparing with just redshift information, in Figure 4 we see that the constraints on A_g and Γ remain largely unchanged and there is a slight improvement in the constraint on β . So for this three parameter set there is relatively little improvement. This is because the inclusion of the velocity data does nothing to break the main degeneracy between A_g and Γ . The other parameters were relatively uncorrelated. The lower panel in Figure 10 shows that the correlations remain unchanged from the redshifts-only analysis.

Figure 11 shows the $\Delta \ln(\text{Likelihood}) = -\frac{1}{2}$ likelihood contours about the fiducial maximum likelihood point in a

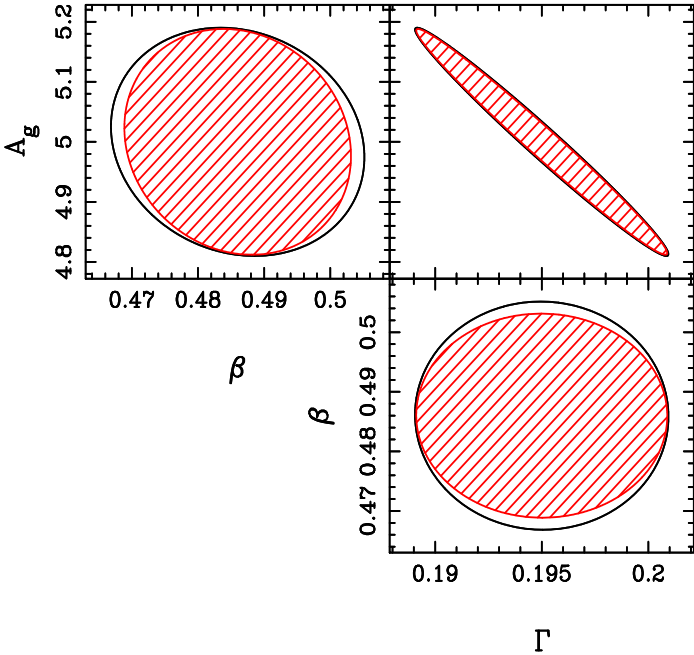


Figure 11. 1σ contours for likelihood marginalised over one free parameter. The outer contour is for the redshift survey only. Hatched regions indicate the constraint from combining with the peculiar velocity survey.

two-parameter space. These contours represent the likelihood marginalised in each case over the one remaining parameter. The outer contour is that from the redshift survey alone whereas the inner hatched region is the constraint when velocity data is included. The maximum wavenumber analysed here is $k = 0.2 h^{-1}\text{Mpc}$.

9.2 Four parameter set

As with the galaxy survey, we can add in a new parameter and study its effect on a likelihood analysis. Adding in ω_b has little effect on A_g and β , but degrades Γ , as was the case for the redshift survey alone. The baryonic density is not detected from the combined survey anyway, nor is the baryon fraction. We shall not consider this set further.

Figure 12 shows the marginalised uncertainties of a four parameter set including the galaxy-mass correlation parameter, r_g . Comparing with Figure 10 we see that A_g and Γ are unchanged by the inclusion of the new parameter, since these are practically independent of r_g . The redshift distortion parameter β , has degraded slightly, due to its strong correlation with r_g , but is still measurable at the 3% level. The big change from the redshifts-only analysis is in the galaxy-mass correlation parameter r_g , which is now measurable from the combined surveys, with a formal uncertainty of better than 2%. Comparing Figure 12 with its redshift-survey-only equivalent Figure 6 it is clear that there has been a great improvement in the joint constraint of β and r_g . The reason for this can be seen by comparing the correlations between the two parameters in the lower panels of both figures. In the redshifts-only analysis β and r_g are

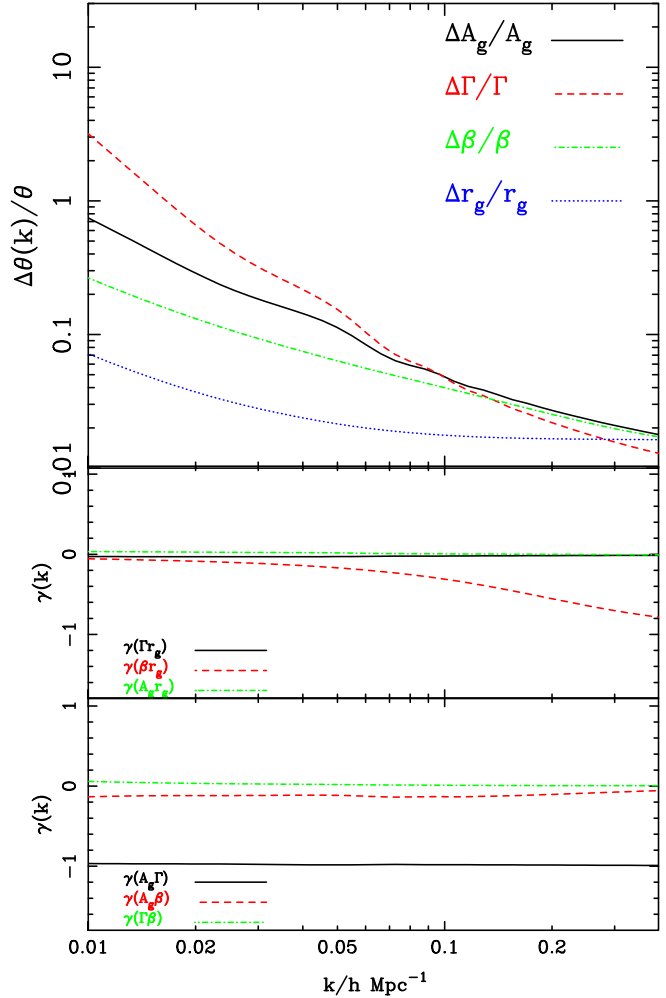


Figure 12. Supermatrix fractional errors and correlations between A_g , Γ , β and r_g .

strongly anticorrelated whereas when the redshifts are combined with peculiar velocities this degeneracy is broken and the parameters become almost independent.

Again we have plotted the expected likelihood contours for this analysis in order to help visualise the improvement in the constraint. In Figure 13 the contours represent $\Delta \ln(\text{Likelihood}) = -\frac{1}{2}$ after marginalization over the two remaining parameters. Again the hatched region shows the improvement from combining the data sets. Particularly interesting is the panel showing contours for β and r_g which illustrates the breaking of the degeneracy between the two, and the subsequent improvement in their joint constraint.

9.3 Scale dependence of b and r_g

Given the tight constraint on r_g and β it is interesting to consider a possible scale dependence in either r_g or the biasing parameter b . Although we have approximated b to be constant over the scale of interest, it may have some scale dependence. Another way to consider scale dependence in the biasing is to fix b as constant and allow the parameter

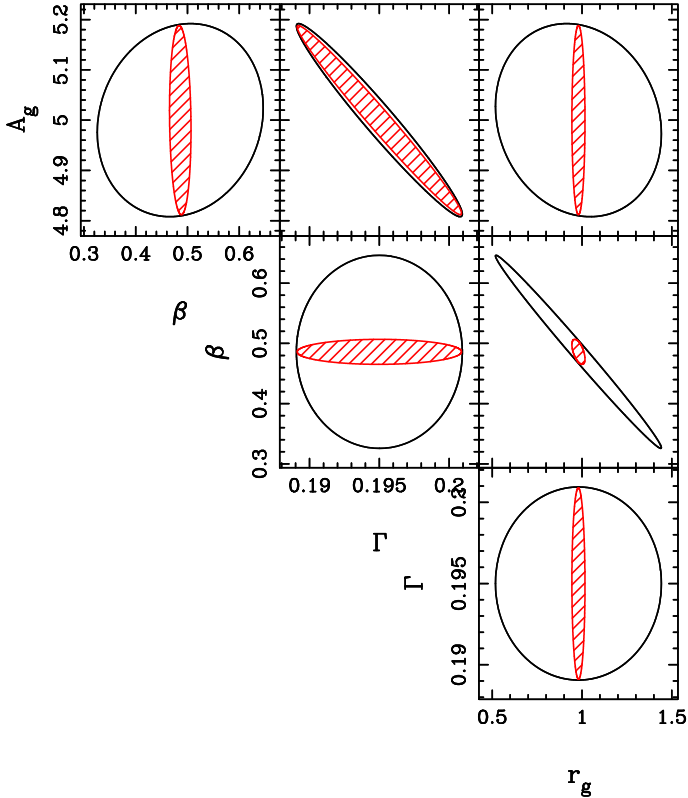


Figure 13. 1σ contours for likelihood marginalised over two free parameters.

r_g to vary with k . The upper panel of Figure (14) shows the expected error bars on a measure of r_g band averaged over a logarithmic passband of width $\Delta \ln k$. The width $\Delta \ln k$ is marked on the plot as a series of dots. b is fixed at $b = 1$ for this analysis. The results are extremely encouraging; $r_g(k)$ can be measured to within about 10% over a wide range of scales improving to 4.5% on the smallest scales. The lower panel shows a similar error bar prediction for estimates of the band -averaged $b(k)$. This plot assumes r_g to be fixed at $r_g = 1$ over all scales. The bias parameter $b(k)$ is even more tightly constrained at a few percent over a wide range.

10 CONCLUSIONS

In this paper we have presented the formalism for the individual and combined Fisher information analysis for galaxy redshift and velocity field surveys. This analysis allows us to optimise both surveys to maximise the information content for cosmological parameters, providing an estimate of the uncertainty on the measurement of the matter and velocity power spectra and the set of cosmological parameters, $(A_g, \Gamma, \beta, \omega_b, r_g)$. For both 6dF redshift and velocity surveys we find the optimal design to be as wide as possible - a result which was previously well known. In the case of the velocity survey we find the best design to be as well sampled and as accurate as possible and in the redshift survey we find an optimal sampling of around 70%. We expect to be able to constrain A_g , Γ and β to around 2 – 3% from the redshift

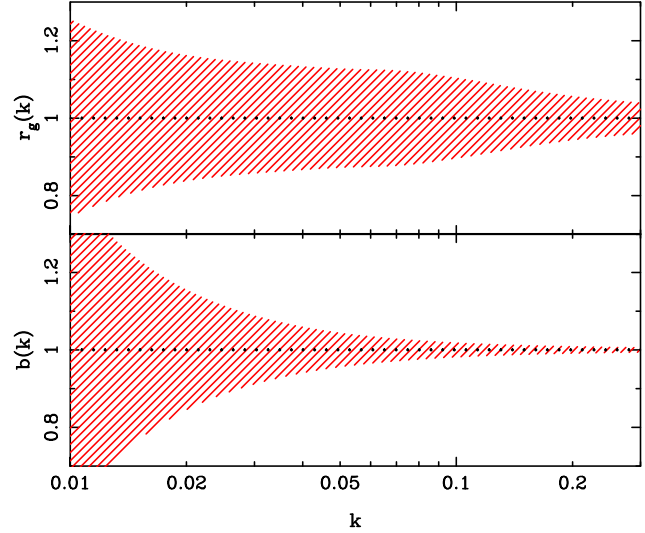


Figure 14. Constraining scale dependence: $\Delta b(k)$ and $\Delta r_g(k)$.

survey. From the velocity survey A_v can be constrained to 5% but a joint constraint of A_v and Γ will have marginalised uncertainties of 25%.

We find that the major benefits of 6dF are found when the velocity and redshift surveys are combined and when we wish to jointly constrain the parameters r_g and β . The parameters' degeneracy is broken when the power spectra are combined and the parameter r_g can be measured much more accurately than in any of the above surveys with just redshifts. Finally, the scale dependence of r_g and b can be measured with the combined data set – which at least will give credence to some of the assumptions commonly made about biasing. Clearly the great benefit of peculiar velocity information is that it tells us about the underlying mass and by combining this information with galaxy redshifts we can learn much about the relationship between luminous and dark matter.

ACKNOWLEDGEMENTS

DB thanks the PPARC for a studentship and ANT thanks the PPARC for an Advanced Fellowship. We also thank Quentin Parker and Will Saunders for invaluable help understanding the 6dF.

11 REFERENCES

- Bouchet, F.R., Prunet, S. and Sethi, S.K. 1999, MNRAS, 302, 663
- Colless, M. et al. 1999, in Looking Deep into the Southern Sky, p9
- Dekel, A. and Lahav, O. 1999, ApJ, 520, 24
- Eisenstein, D.J. and Hu, W. 1998, ApJ, 496, 605
- Feldman, H.A., Kaiser, N. and Peacock, J. A. 1994, ApJ, 426, 23
- Gregg, M. D. 1995, AJ, 110, 1052

- Heavens, A. F. and Taylor, A. N. 1997, MNRAS, 290, 4561
- Jorgensen, I., Franx, M. and Kjaergaard, P. 1993, ApJ, 411, 34
- Kendall, M. G. and Stuart, A. 1969, *The Advanced Theory of Statistics*, Vol 2, Griffin, London
- Kochanek, C. S. et al., 2001, ApJ, 560, 566
- Kolatt, T., et al. 2000, A. S. P. Conf. Ser., 201, 205
- Lawrence, C.R. and Lange A.E. 1997, AAS, 29, 1273
- Peacock, J. A. and Dodds, S. J. 1994, MNRAS, 267, 1020
- Peebles, P. J. E. 1980, *The Large Scale Structure of the Universe*, Princeton University Press, Princeton N.J.
- Skrutskie, M. F. 2000, IAU Symposium, Vol. 204
- Spergel, D. N. et al. 2003, astro-ph/0302209
- Strauss, M. A. and Willick, J. A., 1995, PhR, 261, 271
- Tadros, H. et al. 1999, MNRAS, 305, 527
- Taylor, A. N., Ballinger, W. E., Heavens, A. F. and Tadros, H. 2001, MNRAS, 327, 689
- Taylor, A. N. and Watts, P. I. R. 2001, MNRAS, 328, 1027
- Tegmark, M. 1997, PhRvL, 79, 3806
- Tegmark, M., Taylor, A. N. and Heavens, A. F. 1997, ApJ 480, 22
- Vogeley, M. S. and Szalay, A. S. 1996, ApJ 465, 34
- Wakamatsu, K. et al. in ASP Conf. Ser., IAU 8th Asian-Pacific Regional Meeting, in press astro-ph/0306104
- Zehavi, I. and Dekel, A., in ASP Conf. Ser., 201:Cosmic Flows Workshop
- Zaldarriaga, M., Spergel, D.N. and Seljak, U. 1997, ApJ 488, 1

APPENDIX A: JOINT ESTIMATES OF THE GALAXY CLUSTERING AMPLITUDE, A_g , AND THE REDSHIFT-SPACE DISTORTION PARAMETER, β
A.1 The redshift-space Fisher Matrix

In this Appendix we derive some exact formulae for estimating the uncertainty on a joint measurement of the amplitude of galaxy clustering, A_g , and the redshift distortion parameter, β , in the limit of negligible shot-noise and complete correlation between galaxies and matter, $r_g = 1$, and all other parameters are known. We model the survey volume by an effective constant volume, V . The Fisher matrix in this limit is

$$\mathcal{F}_{ij} = \frac{1}{2}V \int \frac{d^3k}{(2\pi)^3} \partial_i \ln P_{gg}^s(k, \mu) \partial_j \ln P_{gg}^s(k, \mu) \quad (47)$$

where i and j take the values A_g and β .

The galaxy redshifted power spectrum with $r_g = 1$ is given by (c.f. equation (18))

$$P_{gg}^s(\mathbf{k}) = D^2(k\sigma_v\mu)(1 + 2\mu^2\beta + \mu^4\beta^2)b^2P_{mm}(k). \quad (48)$$

Differentiating and angle averaging we find the Fisher matrix is

$$\begin{aligned} \mathcal{F} &= \begin{pmatrix} \mathcal{F}_{A_g A_g} & \mathcal{F}_{\beta A_g} \\ \mathcal{F}_{\beta A_g} & \mathcal{F}_{\beta\beta} \end{pmatrix} \\ &= \begin{pmatrix} 2/A_g^2 & \Phi(\beta)/A_g\beta \\ \Phi(\beta)/A_g\beta & \Theta(\beta)/\beta^2 \end{pmatrix} \frac{k^3 V}{6\pi^2} \end{aligned} \quad (49)$$

where

$$\Theta(\beta) = \int_{-1}^{+1} d\mu \left(\frac{\beta\mu^2}{1 + \beta\mu^2} \right)^2 = 2 + \frac{1}{1 + \beta} - 3 \frac{\tan^{-1} \sqrt{\beta}}{\sqrt{\beta}}, \quad (50)$$

$$\Phi(\beta) = \int_{-1}^{+1} d\mu \left(\frac{\beta\mu^2}{1 + \beta\mu^2} \right) = 2 \left(1 - \frac{\tan^{-1} \sqrt{\beta}}{\sqrt{\beta}} \right) \quad (51)$$

Inverting the Fisher matrix we find the parameter covariance matrix is

$$\begin{aligned} \mathcal{F}^{-1} &= \begin{pmatrix} \langle (\Delta A_g)^2 \rangle & \langle \Delta\beta \Delta A_g \rangle \\ \langle \Delta\beta \Delta A_g \rangle & \langle (\Delta\beta)^2 \rangle \end{pmatrix} \\ &= \begin{pmatrix} A_g^2 \Theta(\beta) & -A_g \beta \Phi(\beta) \\ -A_g \beta \Phi(\beta) & 2\beta^2 \end{pmatrix} \frac{6\pi^2}{k^3 V \Psi(\beta)} \\ &= \begin{pmatrix} (0.01)^2 A_g^2 & -(0.02)^2 A_g \beta \\ -(0.02)^2 A_g \beta & (0.06)^2 \beta^2 \end{pmatrix} \left(\frac{k}{0.2 \text{ hMpc}^{-1}} \right)^{-3} \left(\frac{V}{10^8 [h^{-1} \text{ Mpc}]^3} \right)^{-1} \end{aligned} \quad (52)$$

where

$$\Psi(\beta) = A_g^2 \beta^2 \text{Det } \mathcal{F} = 2 \left(\frac{1}{1 + \beta} + \frac{\tan^{-1} \sqrt{\beta}}{\sqrt{\beta}} - 2 \frac{[\tan^{-1} \sqrt{\beta}]^2}{\beta} \right) \quad (53)$$

and the approximate numerical results in the last line of equation (52) are for $\beta = 0.5$. From this we can read off the marginalised fractional error on the amplitude of galaxy clustering, $\Delta A_g/A_g = 0.01$, and the distortion parameter, $\Delta\beta/\beta = 0.06$, in the absence of shot-noise. For a single-parameter estimate of β the fractional uncertainty reduces to equation (36).

The correlation coefficient between the redshift-space distortion parameter and the amplitude of clustering in the limit of negligible shot-noise and all other parameters known is

$$\gamma_{A_g\beta} = -\frac{\Phi(\beta)}{\sqrt{2\Theta(\beta)}} \approx -0.78, \quad (54)$$

where the final numerical result is again assuming $\beta = 0.5$.

A.2 The uncertainty on an estimate of the amplitude of mass clustering

Taylor et al (2001) and Tadros et al (1999) proposed that the amplitude of mass clustering can be estimated from redshift surveys, if galaxies are perfectly correlated with mass $r_g = 1$, from

$$Q = (A_g \beta) \Omega_m^{-0.6}. \quad (55)$$

If the errors on A_g and β are similar, then this combination has the advantage that it can be estimated more accurately than either of its parts because it marginalises along the longest eigenvalue of the parameter covariance matrix. We can estimate the uncertainty from this combination as

$$\begin{aligned} \frac{\Delta Q}{Q} &= \sqrt{\frac{\langle (\Delta A_g)^2 \rangle}{A_g^2} + \frac{\langle (\Delta \beta)^2 \rangle}{\beta^2} + 2 \frac{\langle \Delta A_g \Delta \beta \rangle}{A_g \beta}} \\ &= \sqrt{\frac{6\pi^2}{k^3 V} \left(\frac{\Theta(\beta) - 2\Phi(\beta) + 2}{\Psi(\beta)} \right)} \end{aligned} \quad (56)$$

For $\beta = 0.5$ this reduces to

$$\frac{\Delta Q}{Q} = 0.05 \left(\frac{k}{0.2 \text{ hMpc}^{-1}} \right)^{-3} \left(\frac{V}{10^8 (h^{-1} \text{ Mpc})^3} \right)^{-1}. \quad (57)$$

Hence although the projected uncertainties on A_g and β are expected to be 1% and 6%, the fractional uncertainty on the more physical parameter Q , can be determined to 5% from redshift surveys, under the assumptions stated above. This is a better constraint than β but not A_g . Because the error bars in A_g and β are so different, the major axis of the error ellipse does not lie at 45 degrees to the parameter axis and so the marginalisation does not allow Q to be better constrained than both of the independent parameters.

APPENDIX B: THE BIVARIATE FISHER MATRIX FOR TWO CORRELATED GAUSSIAN FIELDS

In this Appendix we explicitly calculate the Fisher matrix for two correlated Gaussian fields. If we label the fields X and Y the Fisher matrix may be written in the general form:

$$\mathcal{F}_{ij} = \int d^3 k d^3 r \sum_{XY} \partial_i C_X [\text{Cov}(C_X C_Y)]^{-1} \partial_j C_Y \quad (58)$$

(Zaldarriaga, Spergel and Seljak 1997). In our case, X and Y can denote gg , $u'u'$ and gu' . We can rewrite equation (58) in a way that isolates an effective volume:

$$\mathcal{F}_{ij} = \int d^3 k \sum_{XY} \partial_i C_X \partial_j C_Y \int d^3 r [\text{Cov}(C_X C_Y)]^{-1} \quad (59)$$

The diagonal components of the spectral covariance matrix are:

$$\text{Cov}(C_{gg}(k, r) C_{gg}(k, r)) = 2[P_{gg}(k) + N_{gg}(r)]^2, \quad (60)$$

$$\text{Cov}(C_{u'u'}(k, r) C_{u'u'}(k, r)) = 2[P_{u'u'}(k) + N_{u'u'}(r)]^2, \quad (61)$$

$$\text{Cov}(C_{u'g}(k, r) C_{u'g}(k, r)) = [(P_{u'g}(k))^2 + (P_{u'u'}(k) + N_{u'u'}(r))(P_{gg}(k) + N_{gg}(r))] \quad (62)$$

with off-diagonal parts

$$\text{Cov}(C_{u'u'} C_{gg}) = 2(C_{gu'})^2, \quad (63)$$

$$\text{Cov}(C_{u'u'} C_{gu'}) = 2C_{gu'}(C_{u'u'} + N_{u'u'}), \quad (64)$$

$$\text{Cov}(C_{gg} C_{gu'}) = 2C_{gu'}(C_{gg} + N_{gg}). \quad (65)$$

The full expression for the bivariate Fisher matrix is then:

$$\begin{aligned}
\mathcal{F}_{ij} = & \int \frac{d^3k}{(2\pi)^3} \int d^3r (C_{u'u'}^2 \partial_i C_{gg} \partial_j C_{gg} + 2C_{gg} C_{u'u'} \partial_i C_{gu'} \partial_j C_{gu'} + C_{gg}^2 \partial_i C_{u'u'} \partial_j C_{u'u'} \\
& - 2C_{u'u'} C_{gu'} [\partial_i C_{gu'} \partial_j C_{gg} + \partial_i C_{gg} \partial_j C_{gu'}] \\
& - 2C_{gg} C_{gu'} [\partial_i C_{gu'} \partial_j C_{u'u'} + \partial_i C_{u'u'} \partial_j C_{gu'}] \\
& + C_{gu'}^2 [\partial_i C_{u'u'} \partial_j C_{gg} + 2\partial_i C_{gu'} \partial_j C_{gu'} + \partial_i C_{gg} \partial_j C_{u'u'}]) / (2(C_{gg} C_{u'u'} - C_{gu'}^2)^2)
\end{aligned} \tag{66}$$

where

$$\begin{aligned}
C_{gg} &= P_{gg}(k) + N_{gg}(r), \\
C_{u'u'} &= P_{u'u'}(k) + N_{u'u'}(r), \\
C_{gu'} &= P_{u'g}(k) = r_g \sqrt{P_{gg}(k) P_{u'u'}(k)}.
\end{aligned} \tag{67}$$